

# Microscopy and microanalysis of crystalline glazes

K. M. KNOWLES & F. S. H. B. FREEMAN

University of Cambridge, Department of Materials Science & Metallurgy, Pembroke Street, Cambridge CB2 3QZ, U.K.

**Key words.** Crystalline glazes, gahnite, petrographic analysis, polarized light microscopy, rutile, scanning electron microscopy, willemite, X-ray analysis, X-ray diffraction.

## Summary

Crystalline glazes on ceramic plates produced commercially in the U.K. and on ceramic pots produced commercially in Taiwan and Spain have been examined by X-ray diffraction, conventional and polarized light microscopy, and scanning electron microscopy in order to identify the crystalline phases present in the glazes and to ascertain through X-ray microanalysis the partitioning behaviour of the transition metal ions used to colour the glazes and the crystals within them. In each case examined, the macroscopic two-dimensional spherulites within the glazes clearly seen by the naked eye were found to consist of large numbers of radially orientated acicular crystals each 5  $\mu\text{m}$  or less in width embedded within the silica-rich glaze. Energy dispersive X-ray microanalysis and X-ray diffraction of these crystals identified these crystals as willemite,  $\alpha\text{-Zn}_2\text{SiO}_4$ . The strong [001] texture of these crystals within the glaze evident from the X-ray diffraction patterns was consistent with polarized light microscopy observations of the willemite crystals. In addition to willemite, small iron-doped gahnite ( $\text{ZnAl}_2\text{O}_4$ ) crystals were found in a honey-coloured crystalline glaze and acicular rutile ( $\text{TiO}_2$ ) crystals were found in the Portmeirion Pottery plates examined. Transition metal ions with a preference for tetrahedral coordination were observed to substitute for  $\text{Zn}^{2+}$  ions in willemite and to partition preferentially to the willemite crystals, whereas ions preferring octahedral coordination preferred to remain in the glaze.

## Introduction

Crystalline glazes are devitrified glazes within which spherulites clearly visible to the naked eye that can be 40 mm or more in radius are produced during controlled nucleation and growth processes. While it is believed possible that devitrified

glazes may have first been produced intentionally during the Sung Dynasty in China, it has only been since the 19th century that the ability of glazes to crystallize, and in particular the ability of zinc-containing glazes to crystallize, has been a topic of interest (Creber, 1997). In his 1937 paper on the control of crystalline glazes through careful heat treatment, Norton (1937) noted that there was a considerable body of literature dealing with the composition of the glazes, but very little dealing with the precise temperature schedule required to generate spherulites. Since Norton's paper there have been relatively few references to crystalline glazes in the scientific literature, other than in textbooks on ceramics written or co-written by Norton (Norton, 1970, 1974; Kingery *et al.*, 1976). Norton (1970) noted the lack of petrographic work on crystalline glazes in contrast to the number of papers published showing the wide range of crystals found in crystalline glazes. Indeed, it has only been within the last few years that a significant number of papers on crystalline glazes have emerged in the scientific literature (Goddard, 1995; Sun *et al.*, 1999; Karasu *et al.*, 2000, 2001; Karasu & Turan, 2001, 2002; Rudhovskaya & Mikhailenko, 2001; Turan & Karasu, 2001).

It is apparent from the ceramic art and craft literature that there is an active ceramic glaze community within the pottery world which has clearly adopted the principle of a methodical approach to crystalline glaze formation advocated by Norton and has used this to good effect when imparting practical information on crystalline glaze production (Parmalee & Harman, 1973; Machtey, 1978; Covert, 1981; Schmitz, 1984; Taylor & Bull, 1986; Dann, 1991; Clarkson, 1992; Creber, 1997; Malone, 1997; Ilsley, 1999; von Dassow, 2002; Shimbo, 2003). It is also evident that there is a good practical appreciation of how the incorporation of different transition metal oxides and carbonates into the raw glaze recipes colours the glaze and the spherulites (almost always referred to incorrectly in such literature as 'crystals' or as 'individual crystals' rather than as spherulites) within the glaze (Machtey, 1978; Covert, 1981; Schmitz, 1984; Clarkson, 1992; Creber, 1997; Malone, 1997; Ilsley, 1999; Shimbo, 2003).

Correspondence to: Dr Kevin Knowles. Fax: +44 (0)1223 334567; e-mail: kmk10@cam.ac.uk

The recent work of Karasu and colleagues (Karasu *et al.*, 2000, 2001; Karasu & Turan, 2001, 2002) has been on novel zinc-based crystalline glaze compositions using raw materials native to Turkey, and has shown how standard microstructural characterization techniques such as X-ray diffraction, scanning electron microscopy and X-ray microanalysis can be used to analyse crystalline glazes. In their systems both willemite,  $\alpha$ -Zn<sub>2</sub>SiO<sub>4</sub>, and gahnite, ZnAl<sub>2</sub>O<sub>4</sub>, were routinely found to have crystallised in significant amounts, the latter arising as a direct consequence of the relatively high level of alumina in their starting glaze compositions. These compositions differ from the zinc-based crystalline glaze compositions quoted in the ceramic art and craft literature, which have lower levels of aluminium ions.

In the work described here, and in contrast to the work of Karasu and colleagues, we have chosen deliberately to use microstructural characterization techniques to examine examples of crystalline glazes produced commercially for sale, either as pottery for giftware or, in the case of the Portmeirion Potteries Starfire Collection, intended for both dinnerware and giftware. For each artefact we have prepared samples for optical microscopy (both reflected light and transmitted light), scanning electron microscopy and X-ray diffraction in order to establish unambiguously the nature of the crystalline phases produced and to ascertain the tendency of the transition metal ions used to colour the artefacts either to remain in the glaze or to be incorporated in the crystalline phases.

## Materials and methods

### Materials

Six crystalline glaze artefacts from four different sources were studied (Table 1), chosen to be representative of the range of glaze colours and the variety of spherulite shapes and sizes produced. For convenience these are labelled P1–P6. P1 was purchased from a market stall in Barcelona and is believed to have originated from the Catalunya region of Spain. Samples P2–P5 are from Taiwan, where there is an active pottery industry centred on the town of Yingko near Taipei, which has crystalline glaze pottery as one of its specialities. P6 is from the Starfire Collection produced in the late 1990s and the early

part of the 21st century by Portmeirion Potteries. The Starfire Collection, which is now a discontinued line, consisted of a range of products in three design designations: Jade (dinnerware and giftware), Opal (dinnerware and giftware) and Sapphire (giftware). In each case the principal regions of crystalline glaze were creamy white in colour, but in addition colouring agents were used in the Opal and Sapphire ranges to produce shades of green and blue, respectively, in parts of the crystalline glazes. To contrast with the glazes represented by P1–P5, a plate 19 cm in diameter from the Jade collection was selected for examination as sample P6. No technical information on the heat treatments or glaze starting compositions was provided for any of these samples.

### X-ray diffraction

A Philips PW1730 diffractometer was used in step mode at step times of 5 s for each 0.05° 2 $\theta$  in the angular region 10–120° using Cu K $\alpha$  radiation to examine broken pieces of the various crystalline glaze pots. This diffractometer was also used for a piece of the Portmeirion Potteries plate, but only for the angular region 10–100°. Each piece examined was chosen to be as flat as possible to enable it to be placed into position and held securely in position by Plasticine, with the intention that the X-rays only penetrated the 100–150  $\mu$ m thick surface glaze and not the bodies of the pieces. During the detection and collection of X-rays from these specimens, the normal to the surface of the nominally flat piece of pottery made an angle of 90° –  $\theta$ , with both the incoming and outgoing X-rays at a Bragg angle of  $\theta$ . This enabled the preferred orientation of any crystals within the glaze to be assessed. The inherent curvature of the pots and the distribution of the spherulites on the pots dictated the degree of choice of region from which X-ray diffraction data could be collected, and therefore the quality of the data obtained.

### Optical microscopy

Low magnification reflected light photographs of the spherulites were obtained from the surfaces of each of P1–P5 without any further sample preparation. Samples for transmitted light polarized light optical microscopy of the spherulites

| Artefact  | Spherulite colour | Maximum spherulite radius (mm) | Spherulite morphology | Glaze colour |
|-----------|-------------------|--------------------------------|-----------------------|--------------|
| Pot, P1   | Dark blue         | 5                              | Spiky                 | Blue-grey    |
| Pot, P2   | Rich blue         | 15                             | Circular              | Pale blue    |
| Pot, P3   | Very pale green   | 25                             | Circular              | Turquoise    |
| Pot, P4   | Deep indigo       | 15                             | Mostly circular       | Orange-brown |
| Pot, P5   | Cream             | 8                              | Variable              | Honey        |
| Plate, P6 | Buttermilk        | 20                             | Feathered             | White        |

**Table 1.** Details of the spherulite sizes, shape and colour and the glaze colour for each crystalline glaze artefact.

were obtained by slicing the samples into blocks typically  $3\text{ mm} \times 3\text{ mm} \times$  the ceramic body thickness, so that within each block there were parts of spherulites in the surface glaze. These samples were stuck glaze side down onto pieces of microscope slide, themselves stuck to glass blocks, and were then ground down on silicon carbide paper so that the ceramic body of the sample was ground away, leaving only the glaze. The samples, typically  $100\text{--}150\text{ }\mu\text{m}$  thick at this stage of the specimen preparation process, and with a slightly curved surface on the side of the glaze originally stuck down to the microscope slide, were further ground down on either one or both sides, prior to final polishing using  $6\text{ }\mu\text{m}$  and  $1\text{ }\mu\text{m}$  diamond paste. For each artefact, the primary aim of this specimen preparation procedure was to achieve samples for the transmitted light polarized light microscope sufficiently thin so that, where possible, individual crystals within the glaze could be distinguished in the microscope. Final specimen thicknesses were all comparable with the  $30\text{ }\mu\text{m}$  standard for mineralogical thin sections (Battey, 1981).

#### Scanning electron microscopy

A JEOL-5800LV scanning electron microscope equipped with windowless X-ray microanalysis (EDX) facilities was used at 15 kV. Broken pieces of P1–P5 were carbon coated prior to examination without any further specimen preparation process, while a piece of P6 was examined uncoated in low vacuum mode at a pressure of 32 Pa. Microanalysis was conducted in spot mode.

### Experimental results

#### Visual examination

Photographs of pots P3, P4 and P5 and an Opal plate from the Portmeirion Starfire Collection are shown in Fig. 1. The characteristic spherulitic morphology of the crystalline phase present within the crystalline glaze is evident on each of these three pots. The glaze on the Opal plate is also a crystalline glaze, but here the individual crystalline regions interpenetrate to such an extent that the spherulitic morphology is less evident and instead the crystalline regions have a feather-like fanning appearance more reminiscent of ice crystals frozen on window panes during a hard frost. This was also true for the Jade plate used for the subsequent microstructural work. Reflected light micrographs of spherulites from P1–P5 are shown at slightly higher magnification in Fig. 2. The spherulites on P2–P4 were more circular in nature than those on either P1 or P5, with those on P1 being the most spiky. A relatively wide ring or halo comprising much paler crystals  $\approx 1\text{ mm}$  wide was observed around the spherulites on P3. Similar, narrower haloes were seen around the spherulites on the other four pots. It was usual for the spherulites to make the pots less smooth to the touch than conventionally glazed pottery – this

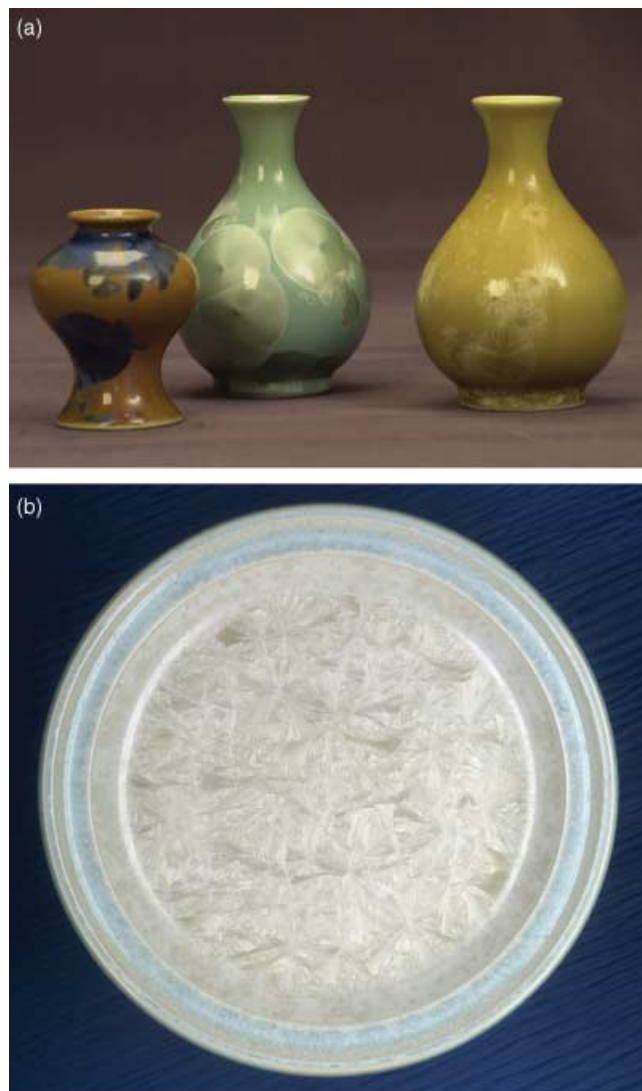


Fig. 1. (a) Pots P3 (centre), P4 (left) and P5 (right), as received and (b) a 19 cm diameter plate from the Opal design in the Portmeirion Starfire Collection. P3 and P5 were 13 cm in height and P4 was 9 cm in height.

was most noticeable for P5 and P1. However, by comparison, the Portmeirion plates felt significantly less smooth to the touch, although there were large variations in smoothness from plate to plate in both the Jade and Opal ranges.

#### X-ray diffraction

An X-ray diffractometer trace from P1 is shown in Fig. 3. A characteristic amorphous hump within the  $20\text{--}30^\circ$   $2\theta$  range is seen, together with sharp diffraction peaks. For  $2\theta < 90^\circ$ , the sharp diffraction peaks could all be indexed as willemite peaks,  $\alpha\text{-Zn}_2\text{SiO}_4$  (trigonal, space group  $R\bar{3}$  (No. 148), hexagonal axes:  $a = 13.948\text{ }\text{\AA}$ ,  $c = 9.315\text{ }\text{\AA}$ ), by comparison with the relevant JCPDS files, 37–1485 and 70–1235. No evidence



Fig. 2. (a)–(e) Reflected light micrographs of spherulites in P1–P5, respectively. The scale bar for all the micrographs shown in (b) is 5 mm. The spherulites in (a) are at the edge of an as-received broken piece from P1. This edge runs from the middle of the right-hand side of (a) to near the bottom left-hand corner of (a).

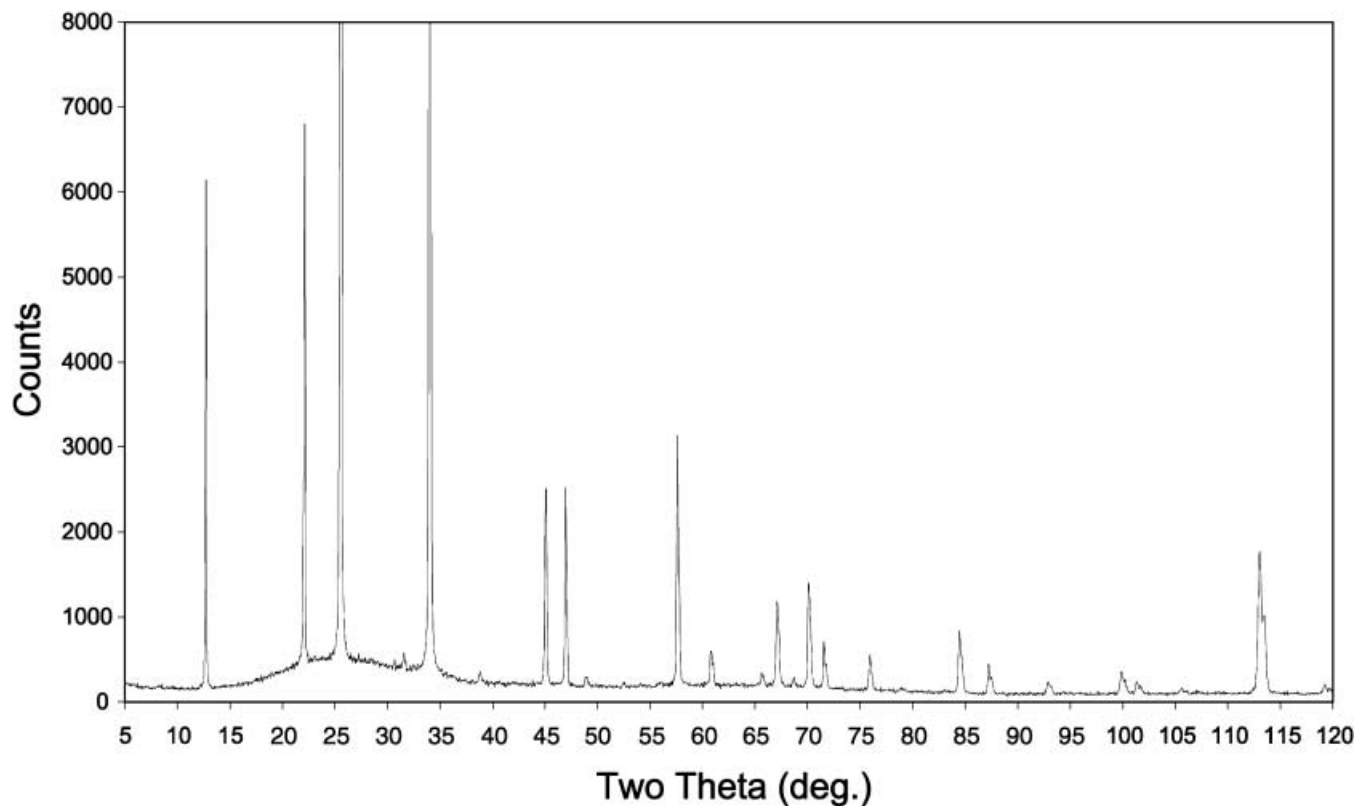


Fig. 3. X-ray diffractometer trace from P1.

**Table 2.** Experimental X-ray diffractometer data from P1. The peaks are indexed for willemite,  $\alpha$ -Zn<sub>2</sub>SiO<sub>4</sub> (JCPDS files 37–1485 and 70–1235).

| Peak position<br>(2 $\theta$ ) | Relative<br>Intensity (%) | <i>h k l</i>     |
|--------------------------------|---------------------------|------------------|
| 12.74                          | 11.9                      | 1 1 0            |
| 22.13                          | 13.1                      | 3 0 0            |
| 25.59                          | 97.6                      | 2 2 0            |
| 31.56                          | 0.4                       | 1 1 $\bar{3}$    |
| 34.06                          | 100.0                     | 4 1 0            |
| 38.82                          | 0.3                       | 2 2 $\bar{3}$    |
| 45.07                          | 4.9                       | 6 0 0            |
| 47.00                          | 4.2                       | 2 5 0            |
| 48.95                          | 0.2                       | 3 3 $\bar{3}$    |
| 57.63                          | 5.3                       | 1 7 0            |
| 60.82                          | 0.8                       | 3 6 0            |
| 65.64                          | 0.3                       | 1 7 $\bar{3}$    |
| 67.11                          | 2.1                       | 5 5 0            |
| 68.70                          | 0.3                       | 6 3 $\bar{3}$    |
| 70.12                          | 2.6                       | 9 0 0            |
| 71.57                          | 1.1                       | 2 8 0            |
| 75.94                          | 0.9                       | 7 4 0            |
| 84.47/84.73                    | 1.5/0.8                   | 10 1 0           |
| 87.26                          | 0.7                       | 3 9 0            |
| 92.90                          | 0.3                       | 5 8 0            |
| 99.90                          | 0.5                       | 12 0 0           |
| 101.35                         | 0.3                       | 11 2 0 and 7 7 0 |
| 105.59                         | 0.1                       | 10 4 0           |
| 113.05/113.44                  | 3.4/1.9                   | 9 6 0            |
| 119.25                         | 0.2                       | 13 1 0           |

was found for any other of the less stable Zn<sub>2</sub>SiO<sub>4</sub> polymorphs reported in the literature (Williamson & Glasser, 1964; Lee *et al.*, 1989). From the analysis of the willemite peaks it became apparent that all the major peaks for  $2\theta < 90^\circ$  were all of the form  $hk0$ . Peaks observed within the range  $90^\circ < 2\theta < 120^\circ$  outside the range of  $2\theta$  specified in the JCPDS files could also be indexed as allowed  $hk0$  willemite reflections (i.e. reflections for which  $-h + k = 3n$  for integer  $n$ ). This was achieved by calculating the relevant  $2\theta$  values and estimating the intensities of the allowed  $hk0$  reflections in this range using a short Excel program. For these estimates, the structure refinement for willemite proposed by Klaska *et al.* (1978), the atomic scattering factors for O, Si and Zn computed using data in Table 6.1.1.4 of the International Tables for Crystallography (Wilson, 1995), the relevant Lorentz polarization factor for each reflection and their multiplicities were all used to compute a relative intensity for each allowed  $hk0$  reflection from a random powder of willemite up to  $2\theta = 120^\circ$ . For simplicity in these calculations a temperature factor of  $0.5 \text{ \AA}^2$  was assumed for each atom.

The indexing of the willemite peaks in Fig. 3 is summarized in Table 2. Each peak position quoted in Table 2 is of the order of  $0.05^\circ$  higher than the value of  $2\theta$  quoted in the JCPDS file

37–1485. These differences are most likely to be due to small errors introduced into the diffraction measurement process through the experimental set-up that we used. Doublets seen at higher Bragg angles such as at the 10 1 0 and 9 6 0 reflections have their individual experimental intensities assigned. It is significant that the  $hkl$  peaks are almost entirely suppressed by comparison with the JCPDS files 37–1485 and 70–1235. Hence, for example, the  $11\bar{3}$  peak at  $2\theta = 31.53^\circ$  on JCPDS file 37–1485, which experimentally is the most intense willemite peak from a randomly orientated powder sample, and which can be identified as the peak in Fig. 3 at  $2\theta = 31.56^\circ$ , barely rises above the background. Thus, it can be deduced that the willemite crystals within the glaze have a strong preferred orientation, so that for each crystal the [001] direction lies parallel to the surface of the crystalline glaze. Hence, in the experimental set-up we have used here, only  $hk0$  reflections will be strong. This preferred orientation determined directly by X-rays using a relatively straightforward experimental set-up and specimen preparation procedure accords with the texture for willemite in crystalline glazes reported by Karasu and coworkers. It is therefore possible to infer that they recorded X-ray diffractometer traces from bulk samples, rather than from powdered samples taken from the bulk glaze. Dr Karasu (personal communication, 2004) has confirmed that this was indeed the case.

X-ray diffraction of pots P2–P5 also showed strong  $hk0$  peaks from willemite characteristic of the [001] directions of the individual willemite crystals lying in the surface of the crystalline glaze. In addition, weak peaks typically with intensities of at most 1–2% of the most intense peaks were found, but the presence or absence of such peaks seemed to differ between diffractometer traces from the same pot. Therefore, these peaks were not thought to arise unambiguously from the crystalline glaze. Klaska *et al.* (1978) quote a mass absorption coefficient,  $\mu$ , for willemite of  $197.3 \text{ cm}^{-1}$  for Cu K $\alpha$  radiation and the effect of absorption on intensities seen in X-ray diffractometer traces is discussed by Cullity & Stock (2001). A simple calculation shows that for a Bragg angle of  $45^\circ$ , the thickness that a specimen of pure willemite must be in order that the intensity diffracted from a thin layer on the back of the specimen is 0.001 of the intensity diffracted by a thin layer on the front of the specimen is  $124 \text{ }\mu\text{m}$ . This value will increase if pure willemite is replaced in such a calculation by a mixture of willemite and glaze, principally because the glaze has a lower density than willemite. Hence, it is entirely possible that the aforementioned weak peaks do not arise unambiguously from the crystalline glaze and can come from the body of the pots. Variations in the intensities of the strongest  $hk0$  peaks seen when comparing the data from P1–P5 could be rationalized in terms of the finite numbers of crystals contributing to the intensities of each  $hk0$  diffraction peak by comparison with an

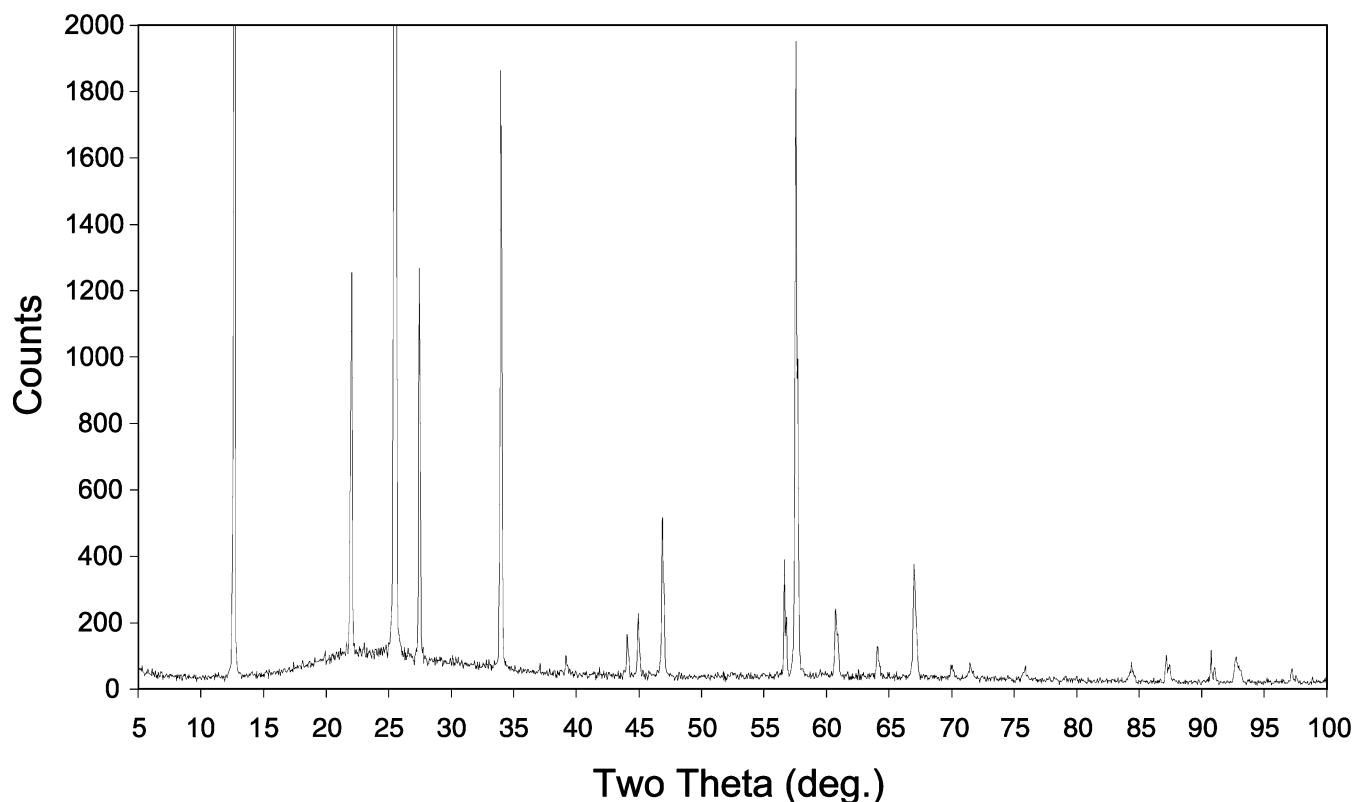


Fig. 4. X-ray diffractometer trace from P6.

ideal textured sample in which there are a very large number of crystals with their [001] directions in the plane of a flat powder bed surface.

The X-ray diffractometer trace from P6 shown in Fig. 4 was significantly different from those from P1–P5. In addition to the  $hk0$  reflections from willemite, a strong reflection occurs at  $2\theta = 27.46^\circ$ , with further weaker peaks at higher Bragg angles. These additional peaks all index satisfactorily as  $hk0$  reflections from rutile,  $\text{TiO}_2$  [tetragonal, space group  $P4_2/mnm$  (No. 136),  $a = 4.594 \text{ \AA}$ ,  $c = 2.9589 \text{ \AA}$ , JCPDS file 87–0920]. The indexing of the peaks in Fig. 4 is summarized in Table 3. Hence, in P6, X-ray diffractometry shows directly not only the willemite peaks and texture expected from the data obtained from P1–P5, but in addition rutile crystals, also with a characteristic texture where their [001] directions lie parallel to the crystalline glaze surface.

#### Transmitted light polarized light microscopy

Examples of observations made with a sensitive tint plate are shown in Fig. 5. Parts of willemite spherulites and glaze alone are seen in Fig. 5(a)–(d), whereas in Fig. 5(e) and (f) additional features are seen. The fibrous nature and the radial texture of the spherulites are apparent, most noticeably in Fig. 5(b) and (c). It is evident from these micrographs that, when the axes of the acicular (needle-shaped) crystals giving rise to the fibrous nature of the spherulites are aligned parallel to the

slow direction of the sensitive tint, the optical path difference increases, so that the interference colour seen on a Michel–Lévy chart (Battey, 1981; Cox *et al.*, 1988) moves to a second-order blue, or higher, depending on how many acicular willemite crystals occur through the thickness of the sample at the position of interest. Willemite is optically positive (Ehringhaus & Rose, 1923; Gaines *et al.*, 1997) with  $n_o = 1.6893$  and  $n_e = 1.7179$  and a birefringence of 0.0286 at the wavelength of sodium *D* light reported from a mineralogical sample found near Aachen (Ehringhaus & Rose, 1923). Since it has been shown from the X-ray diffraction experiments that the [001] directions of the willemite crystals lie within the surface of the glaze, the polarized light micrographs in Fig. 5 confirm that the axes of the acicular willemite crystals within the spherulites must be [001] willemite directions. This is in agreement with the texture quoted in the literature (Sun *et al.*, 1999) and the trigonal nature of the willemite unit cell.

Direct measurement of the width of the individual acicular needles seen most easily in Fig. 5(d) suggests that their width is typically 2–3  $\mu\text{m}$  and at most 5  $\mu\text{m}$ . If it is further assumed that the width of the needles is the same as their depth seen in the polarized light microscope, then the additional optical path difference that would be introduced by a single acicular crystal orientated with its slow direction parallel to the slow direction of the sensitive tint would be of the order of  $0.0286 \times 5000 \text{ nm} = 143 \text{ nm}$ . This is consistent with the

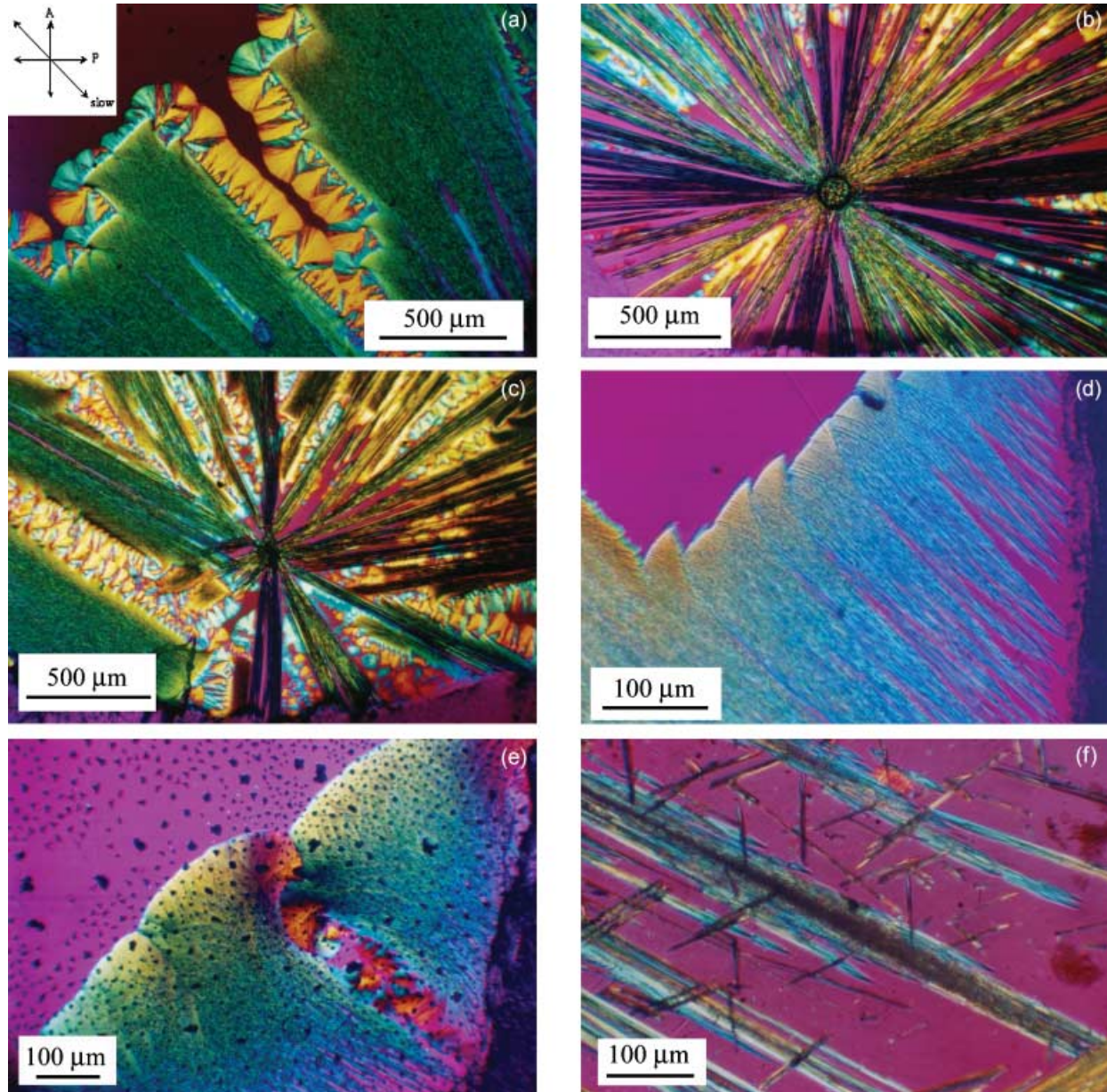


Fig. 5. Polarized light micrographs of crystalline glazes taken with crossed polars and a sensitive tint plate. In each micrograph the extinction directions are horizontal and vertical. The sensitive tint plate was inserted at  $45^\circ$  to the extinction directions. (a) A spherulite–glaze interface from P1. The glaze is at the top left of this micrograph and as it is isotropic, it has the sensitive tint colour under these imaging conditions. Copious secondary spherulitic crystallization, predominantly first-order yellow in colour but also showing the sensitive tint colour and second-order blue, can be seen at this interface within which it is not possible to identify individual crystals. The average axis direction of the needle-shaped crystals within the spherulite is aligned parallel to the slow direction of the sensitive tint plate. The inset shows the extinction directions P and A and the slow direction of the sensitive tint for this and the other polarized light micrographs. (b) and (c) Details of the centre of spherulites from P1. Note that there are regions of glaze between bundles of acicular willemite crystals. In both these micrographs small regions of glue are visible in the bottom parts of the micrographs. (d) Detail of a spherulite–glaze interface in P4 with the average axis direction of the needle-shaped crystals within the spherulite aligned parallel to the slow direction of the sensitive tint plate. A small region of glue is visible on the right-hand side of this micrograph. (e) Detail of a spherulite–glaze interface in P5 with the average axis direction of the needle-shaped crystals within the spherulite aligned parallel to the slow direction of the sensitive tint plate. The occurrence of additional smaller, optically isotropic, features a few micrometres in size is apparent both in the spherulite region and in the glaze. A small region of glue is visible on the right-hand side of this micrograph. (f) Detail of the glaze in P6 showing a bimodal distribution of crystals, the larger crystals showing similar optical behaviour to those seen in P1–P5 and the smaller crystals showing markedly higher birefringence and very high relief. Here the average axis direction of the longer needle-shaped crystals is not quite parallel to the slow axis of the sensitive tint, as the aim was to obtain good quality contrast from both sets of crystals.

**Table 3.** Experimental X-ray diffractometer data from P6. The peaks can be indexed to willemite,  $\alpha$ -Zn<sub>2</sub>SiO<sub>4</sub> (JCPDS files 37–1485 and 70–1235) and rutile, TiO<sub>2</sub> (JCPDS files 83–2242 and 87–0920).

| Peak position (2 $\theta$ ) | Relative intensity (%) | Willemite |          |          | Rutile   |          |          |
|-----------------------------|------------------------|-----------|----------|----------|----------|----------|----------|
|                             |                        | <i>h</i>  | <i>k</i> | <i>l</i> | <i>h</i> | <i>k</i> | <i>l</i> |
| 12.67                       | 24.7                   | 1         | 1        | 0        |          |          |          |
| 22.02                       | 8.8                    | 3         | 0        | 0        |          |          |          |
| 25.53                       | 100.0                  | 2         | 2        | 0        |          |          |          |
| 27.46                       | 10.5                   |           |          |          | 1        | 1        | 0        |
| 33.98                       | 14.8                   | 4         | 1        | 0        |          |          |          |
| 39.19                       | 0.5                    |           |          |          | 2        | 0        | 0        |
| 44.10                       | 1.0                    |           |          |          | 2        | 1        | 0        |
| 44.96                       | 1.6                    | 6         | 0        | 0        |          |          |          |
| 46.91                       | 4.1                    | 2         | 5        | 0        |          |          |          |
| 56.63                       | 3.2                    |           |          |          | 2        | 2        | 0        |
| 57.53                       | 16.8                   | 1         | 7        | 0        |          |          |          |
| 60.72                       | 1.9                    | 3         | 6        | 0        |          |          |          |
| 64.08                       | 0.8                    |           |          |          | 3        | 1        | 0        |
| 67.00                       | 3.0                    | 5         | 5        | 0        |          |          |          |
| 69.99                       | 0.2                    | 9         | 0        | 0        |          |          |          |
| 71.49                       | 0.4                    | 2         | 8        | 0        |          |          |          |
| 75.86                       | 0.3                    | 7         | 4        | 0        |          |          |          |
| 84.35                       | 0.5                    | 10        | 1        | 0        | 4        | 0        | 0        |
| 87.12                       | 0.6                    | 3         | 9        | 0        |          |          |          |
| 90.74/91.03                 | 0.9/0.4                |           |          |          | 3        | 3        | 0        |
| 92.73                       | 0.7                    | 5         | 8        | 0        |          |          |          |
| 97.19                       | 0.4                    |           |          |          | 4        | 2        | 0        |

second-order blue colour seen from the acicular crystals in Fig. 5(d) away from the spherulite–glaze interface.

Features additional to the willemite crystals are shown in Fig. 5(e) and (f). In Fig. 5(e) there are small, optically isotropic, micrometre-sized features over the whole of the crystalline glaze. These features can also be seen on the original pot with a 7 $\times$  optical eyepiece and are integral to the development of the crystalline glaze in P5. The additional features in P6 seen in Fig. 5(f) are the acicular rutile crystals, noticeably smaller

than the acicular willemite crystals. Rutile is also optically positive, but has an extreme birefringence of 0.287 (Battey, 1981), and so the optical path difference introduced by light passing through rutile crystals is an order of magnitude greater than for the willemite crystals, thus making the use of the sensitive tint not relevant for the rutile crystals. Natural rutile is reported to occur as needle-like crystals (Deer *et al.*, 1966; Battey, 1981) and from straightforward crystallographic considerations the axes of the needles will be [001]. This is also consistent with the results of the X-ray diffraction work on P6 discussed in the previous section.

#### Scanning electron microscopy

Visual examination of the pieces of P1–P6 in the scanning electron microscope confirmed aspects of the morphologies of the spherulites within the crystalline glaze evident using polarized light transmitted light microscopy, such as the haloes at the edges of the spherulites and the additional features seen in P5 (Fig. 6). For each artefact, energy dispersive X-ray microanalysis was used in spot mode to measure the glaze compositions and the compositions of the willemite crystals. In addition, energy dispersive X-ray microanalysis was used on P5 to examine the features seen in the polarized light microscope and on P6 to detect rutile crystals. As Goodhew *et al.* (2001) note, it is difficult to make the interaction volume for X-rays smaller than 1  $\mu\text{m} \times 1 \mu\text{m} \times 1 \mu\text{m}$  in a scanning electron microscope, and so it was recognized that our microanalysis results would have to be interpreted with this in mind, particularly when analysing the features on P5 and the rutile crystals on P6.

If the crystals within the spherulites were willemite crystals of stoichiometric composition, the composition detected by energy dispersive X-ray microanalysis would be Zn 28.6 at%, Si 14.3 at% and O 57.1 at%. As an example of the quality of data obtained, measurements of the compositions of the willemite crystals and the glaze from P1 with the carbon signal removed are shown in Table 4. These data arise from five spot

| Element | Willemite crystals     |                          | Glaze                  |                          |
|---------|------------------------|--------------------------|------------------------|--------------------------|
|         | Mean composition (at%) | Standard deviation (at%) | Mean composition (at%) | Standard deviation (at%) |
| O       | 60.44                  | 4.58                     | 68.17                  | 0.97                     |
| Al      | 0.30                   | 0.11                     | 4.48                   | 0.19                     |
| Si      | 12.99                  | 0.74                     | 19.33                  | 0.71                     |
| S       | 0.03                   | 0.02                     | 0.04                   | 0.02                     |
| K       | 0.1                    | 0.05                     | 1.58                   | 0.21                     |
| Ca      | 0.04                   | 0.06                     | 1.81                   | 0.31                     |
| Ti      | 0.13                   | 0.07                     | 1.03                   | 0.09                     |
| Zn      | 25.59                  | 4.06                     | 3.48                   | 0.65                     |
| Co      | 0.38                   | 0.06                     | 0.09                   | 0.02                     |

**Table 4.** Compositional analyses of the willemite crystals and the glaze in P1 determined by EDX microanalysis.

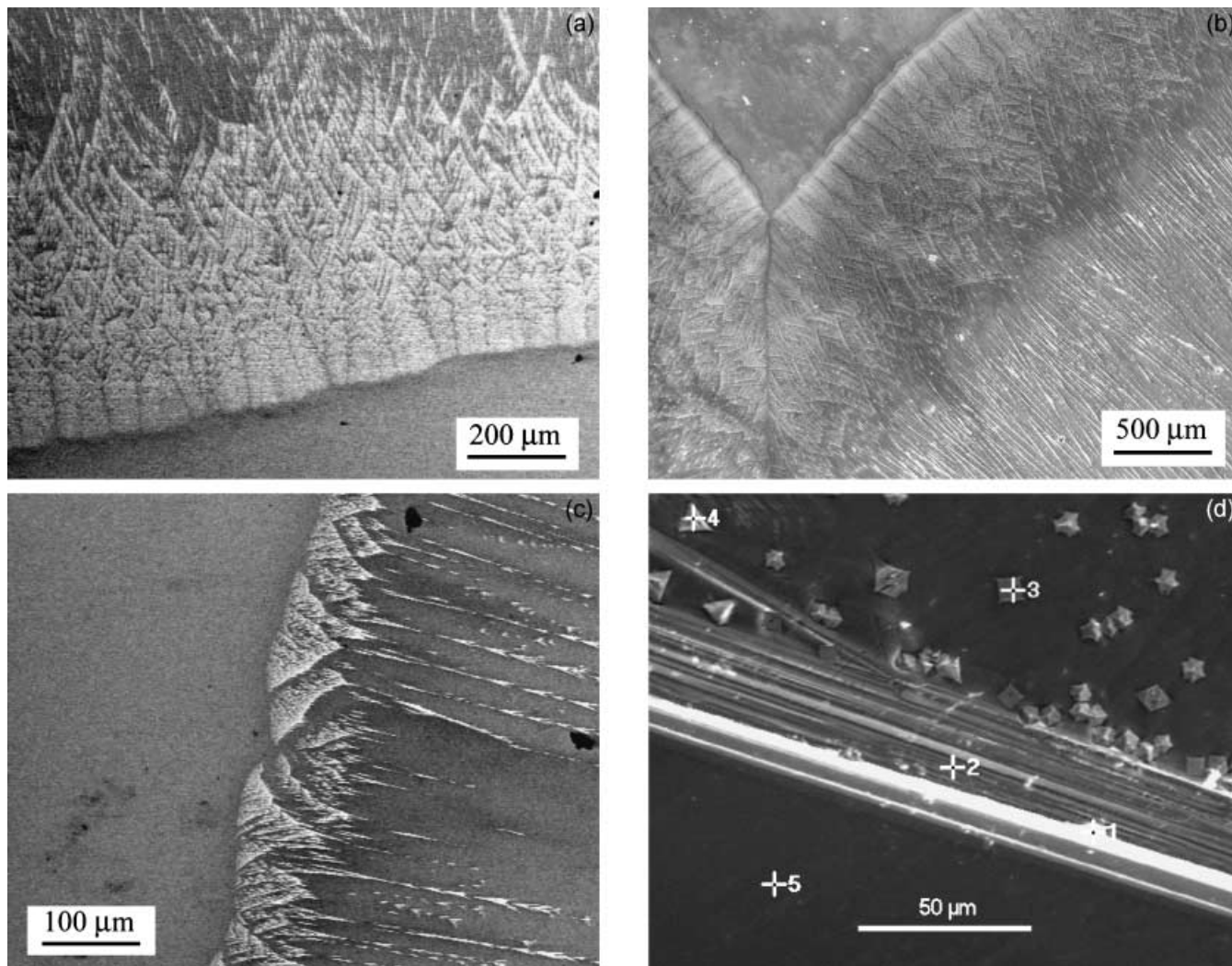


Fig. 6. Scanning electron microscope secondary electron micrographs of crystalline glazes: (a) from P2; (b) from P3; (c) from P4; and (d) from P5. In (d) the areas used for compositional analysis are indicated by the numbers 1–5.

analyses on willemite crystals and four spot analyses on the glaze. Making allowance for experimental measurement error, and in particular for the possible incorporation of glaze into the interaction volume sampled by the electron beam when analysing the willemite crystals, it is apparent that the composition given for the willemite is in accord with expectations. It is also apparent that the composition of the willemite is significantly different from that of the remnant glaze. There is partitioning between the crystal and the glaze not only of O, Si and Zn, but also minor chemical constituents. Ignoring the presence of sulphur, which is not expected in the glaze and is most likely an artefact of the data analysis, it is apparent that Al, K, Ca and Ti remain preferentially in the glaze, whereas Co clearly segregates to the willemite.

Chemical analyses of the other pots P2–P5 confirmed the general trends seen in P1. Al, K and Ca remain in the glaze in P2–P5, whereas the proportions of O, Si and Zn in the crystals

reflect the fact that they are willemite. Microanalysis of the colorant transition metal ions in the willemite and the glaze of each pot is summarized in Table 5 and the proportions of Ti levels in the willemite and the glaze are summarized in Table 6. It would appear from the Ti levels in Table 6 that Ti was only added intentionally to the glaze compositions of P1 and P4.

Analysis of the rutile crystals within the Portmeirion plate showed dramatically the effect of the sampling volume being greater than the volume of crystal under observation (Fig. 7). The accepted  $\text{SiO}_2$ – $\text{TiO}_2$  phase diagram (Levin *et al.*, 1964) shows that rutile does not dissolve silica at all, and so we can confidently expect that the crystals identifiable by energy dispersive X-ray microanalysis as rutile by virtue of their high titanium content will be free of silicon. However, quantitative analysis of the energy dispersive X-ray microanalysis from spots 1 and 2 show Si levels of 15.1 and 18.7 at%, respectively,

**Table 5.** Mean compositional analyses of the colorant transition metal ions in the willemite crystals and the glaze in P1–P5 determined by EDX microanalysis.

| Pot | Willemite crystals |                        | Glaze   |                        |
|-----|--------------------|------------------------|---------|------------------------|
|     | Element            | Mean composition (at%) | Element | Mean composition (at%) |
| P1  | Cobalt             | 0.38                   | Cobalt  | 0.09                   |
| P2  | Cobalt             | 0.10                   | Cobalt  | 0.00                   |
| P3  | Copper             | 0.49                   | Copper  | 0.71                   |
| P4  | Nickel             | 0.93                   | Nickel  | 0.40                   |
| P4  | Iron               | 0.11                   | Iron    | 0.28                   |
| P5  | Iron               | 0.36                   | Iron    | 0.69                   |

**Table 6.** Mean level of titanium metal ions in the willemite crystals and the glaze in P1–P5 determined by EDX microanalysis.

| Pot | Level of titanium in the willemite crystals (at%) | Level of titanium in the glaze (at%) |
|-----|---|--------------------------------------|
| P1  | 0.13  | 1.03                                 |
| P2  | 0.01  | 0.04                                 |
| P3  | 0.04  | 0.02                                 |
| P4  | 0.09  | 0.48                                 |
| P5  | 0.02  | 0.07                                 |

in comparison with the Ti levels recorded of 8.4 and 5.8 at%, respectively. It is also evident from the scale of the back-scattered electron image in Fig. 7(a) that within the regions seen by the naked eye as crystal, there is a significant amount of glass coexisting with the rutile crystals and the willemite crystals. Ti levels recorded in the glaze averaged 1.3 at%. In sharp contrast to P1 and P4, comparable levels of Ti were also recorded in the willemite crystals (see, for example, Fig. 7d), but this could well be an artefact arising from the effect of sampling volume and the intimate mixing in P6 of glaze, willemite and rutile across the entire crystalline glaze region of the plate.

Analysis of the small optically isotropic micrometre-sized features in P5 such as points 3 and 4 in Fig. 6(d) showed that they contained increased levels of iron and aluminium relative to both the willemite (points 1 and 2) and the glaze (point 5). However, significant levels of Si were also recorded from these two particles: 4.4 at% from point 3 and 10.9 at% from point 4. A larger feature with the same morphology recorded a much lower level of Si of 0.2 at%, with 20.6 at% Al, 15.7 at% Zn, 5 at% Fe and 58.5 at% O. That these features are isotropic between crossed polars suggests that these crystals are gahnite,  $\text{ZnAl}_2\text{O}_4$  (cubic, space group  $Fd\bar{3}m$  (No. 227),  $a = 8.0848 \text{ \AA}$ , JCPDS file 05–0669) into which Fe ions have been incorporated.

Gahnite has the spinel structure (Deer *et al.*, 1966). Fe can be incorporated in the gahnite structure as either  $\text{Fe}^{2+}$  or  $\text{Fe}^{3+}$ , substituting either for  $\text{Zn}^{2+}$  or  $\text{Al}^{3+}$  ions, respectively (Deer *et al.*, 1966; Waerenborgh *et al.*, 1994).

Deer *et al.* (1966) note that in natural gahnites there can be considerable substitution of Fe for Zn, leading to a composition of the general form  $\text{Zn}_x\text{Fe}_{1-x}\text{Al}_2\text{O}_4$ . Complete iron substitution for zinc would give rise to the mineral  $\text{FeAl}_2\text{O}_4$ , hercynite, which also has the spinel structure (Deer *et al.*, 1966). It is therefore entirely feasible for this substitution to occur in P5 to give iron-doped gahnite. Equally possible is that  $\text{Fe}^{3+}$  can substitute for  $\text{Al}^{3+}$  ions, leading to iron-doped gahnites with the general formula  $\text{ZnFe}_y\text{Al}_{2-y}\text{O}_4$ . There is the further intriguing possibility that both  $\text{Fe}^{2+}$  and  $\text{Fe}^{3+}$  can be incorporated into the gahnite structure. The composition of the large feature would appear to be more consistent with the substitution of  $\text{Fe}^{3+}$  for  $\text{Al}^{3+}$ , so that the at% of (Al + Fe) is twice that of Zn. The spot analyses at points 3 and 4, in which the levels of Al, Fe and Zn recorded were 17.8 at%, 4.8 at% and 11.5 at% for point 3 and 15.03 at%, 4.6 at% and 10.4 at% for point 4 are also consistent with this interpretation.

Gahnite crystals were not seen in any of the other pots, and so it would appear that the level of Fe added to the glaze has catalysed the formation of the gahnite crystals in P5. The morphology of these features in P5 is also consistent with the gahnite crystals seen by Karasu and co-workers. A comparison of the X-ray diffractometer traces they obtained with the JCPDS files 05–0669 for gahnite and 82–1038 for  $\text{ZnFe}_{0.2}\text{Al}_{1.8}\text{O}_4$  shows that in their X-ray diffractometer traces the 111 peak at  $2\theta = 18.99^\circ$  is unusually strong, indicative of a strong 111 texture, and that the 220 and 311 peaks at  $31.24^\circ$  and  $36.84^\circ$ , respectively, are significantly much less intense than would be expected from a powder sample, and again consistent with a strong 111 texture. This further confirms that the diffractometer traces of Karasu and co-workers are from bulk samples rather than powders.

However, unequivocal evidence for gahnite was not seen in the X-ray diffractometer traces obtained from P5; although there were some very weak peaks recorded in addition to the willemite peaks which occurred near the peak positions that might be expected for the gahnite, there were other equally very weak peaks which would not have been expected. Moreover, recognizing that the replacement of  $\text{Al}^{3+}$  by  $\text{Fe}^{3+}$  in gahnite will increase the lattice parameter of gahnite to around  $8.16 \text{ \AA}$  using our EDX results and combining these with lattice parameter data from Waerenborgh *et al.* (1994), it was apparent that the actual peak positions which might be expected all shift to lower  $2\theta$  values than in undoped gahnite, making the labelling of the weak peaks clearly inconsistent with iron-doped gahnite. Furthermore, in contrast with the observations of Karasu and co-workers, no gahnite peak, which would be expected at a  $2\theta$  value slightly less than  $18.99^\circ$ , was detectable. The most logical reason for the absence of iron-doped gahnite peaks in the X-ray diffractometer traces is a combination of a

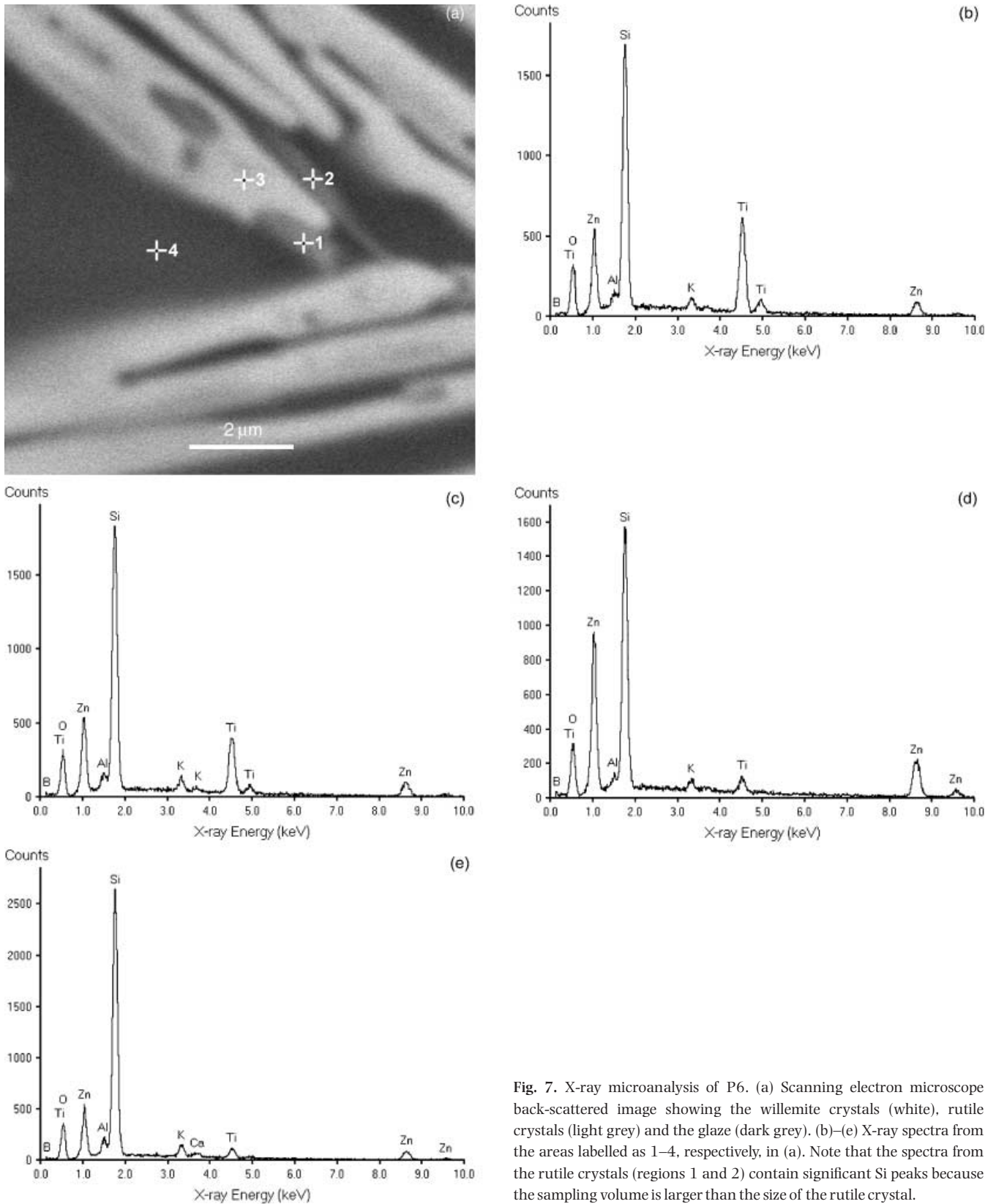


Fig. 7. X-ray microanalysis of P6. (a) Scanning electron microscope back-scattered image showing the willemite crystals (white), rutile crystals (light grey) and the glaze (dark grey). (b)–(e) X-ray spectra from the areas labelled as 1–4, respectively, in (a). Note that the spectra from the rutile crystals (regions 1 and 2) contain significant Si peaks because the sampling volume is larger than the size of the rutile crystal.

111 preferred texture in the gahnite crystals and a lower number of crystals per unit volume than those seen in the glazes examined by Karasu and co-workers.

## Discussion

The combination of X-ray diffraction, optical microscopy and X-ray microanalysis that we have used here enables a consistent picture to emerge about the different crystalline glazes on P1–P6. Apart from the thin sections prepared for transmitted light polarized light microscopy, specimen preparation was deliberately kept minimal. It would be straightforward to adapt the specimen preparation procedure used for the thin sections to the preparation of samples for transmission electron microscopy by dimpling and ion beam thinning.

In each crystalline glaze examined, the macroscopic spherulites have been shown to be willemite,  $\alpha$ -Zn<sub>2</sub>SiO<sub>4</sub>, and in each case the spherulites have been shown to comprise acicular crystals with their axes along [001]. Additional crystallization, such as the formation of iron-doped gahnite in P5 and the formation of rutile crystals in P6, is on a significantly finer scale. Although both of the iron-doped gahnite crystals and the rutile crystals can be seen using a 7 $\times$  optical eyepiece on the glazes of P5 and P6, their fine scale means that an observer using such an eyepiece can easily overlook them.

The haloes seen around the willemite spherulites in P1–P5 comprise numerous finer acicular willemite crystals, as is evident from the polarized light micrographs in Fig. 5 and the secondary electron scanning electron micrographs in Fig. 6. As Creber (1997) notes, such haloes can be generated by temporarily lowering the temperature within the furnace during the heat treatment used to produce the spherulites. From classical nucleation theory, this lowering of temperature has the effect of increasing the rate of heterogeneous nucleation, consistent with Figs 5 and 6, and decreasing the rate of crystal growth (Kingery *et al.*, 1976). The haloes seen in P1–P5 will have been formed at the end of the heat treatment, either through natural cooling after the furnace has been switched off or from a deliberate and steady decrease in temperature of the furnace during the growth of the spherulites (see also, for example, the discussion in Goddard, 1995 and Ilsley, 1999). A good example of heterogeneous nucleation can be seen in Fig. 5(a), where the heat treatment used to make P1 has spawned a halo between the long blue acicular willemite crystals and the glaze, within which there has been copious heterogeneous nucleation and ensuing spherulitic growth, giving rise to the mixture of first-order yellow, sensitive tint colour and second-order blue within these small spherulites.

Stoichiometric willemite is colourless. Colour is imparted to willemite crystals and the surrounding glaze by the transition metal ions deliberately added to the starting glaze composition. As is evident from Table 5, elements such as cobalt and nickel segregate to the willemite, whereas the concentrations of iron and copper are richer in the glaze. Titanium ions

also prefer to remain outside the willemite crystals, and it is apparent from the Portmeirion Potteries Starfire plates that if there is sufficient titanium in the starting glaze composition, crystals of rutile can form in addition to the majority willemite.

Willemite belongs to the phenakite group of minerals of the general formula R<sub>2</sub>SiO<sub>4</sub> (Gaines *et al.*, 1997). The crystal structures of these minerals are based upon a close packing of oxygen anions with all the R and Si cations in tetrahedral coordination. It is therefore reasonable to expect that foreign metal ions which prefer tetrahedral coordination will be able to be incorporated into the willemite structure, whereas metal ions preferring octahedral coordination will be unlikely to be readily incorporated into the willemite structure. Gaines *et al.* (1997) state that Co<sup>2+</sup>, Fe<sup>2+</sup> and Mn<sup>2+</sup> are all known replacements for Zn<sup>2+</sup> in willemite.

Without more detailed calculation, it is immediately apparent that Ti ions are unlikely to be incorporated into the willemite crystal structure. Rutile and anatase, two of the oxides of titanium, and the perovskite family of materials are well-known examples of structures in which titanium ions sit in octahedral sites (Deer *et al.*, 1966; Battey, 1981). Gratifyingly, this is consistent with the results of the X-ray microanalysis for titanium shown in Table 6 from the five pots, although not with the levels of titanium found in the willemite crystals in P6. However, as we have already noted, the X-ray microanalysis results from P6 seemed to have sampled volumes larger than intended.

The way in which colour is imparted to glazes by transition metal elements is specified in a technical manner suitable for ceramic art and craft practitioners by Parmalee & Harman (1973). A more detailed scientific understanding is provided by crystal-field and ligand-field chemistry (Kingery *et al.*, 1976; Paul, 1982; Müller, 1992; Tilley, 2000). Kingery *et al.* (1976) note that, while the colours of ions in silicate glasses depend primarily on the coordination number and oxidation state, changes in oxidation state or the presence of multiple oxidation states can lead to a wide range of colours produced by the same ion in different host glasses.

In both P1 and P2 the colorant is cobalt. The blue colour generated by the willemite crystals is characteristic of Co<sup>2+</sup> ions occupying tetrahedral coordination (Parmalee & Harman, 1973). Here, the Co<sup>2+</sup> ions substitute for the Zn<sup>2+</sup> ions in the willemite crystal structure. By contrast, the very pale blue of the remnant glaze shows that the concentration of cobalt is significantly lower. Here too, the colour blue indicates that Co<sup>2+</sup> ions prefer tetrahedral coordination. The deep indigo of the willemite crystals on P4 can also be rationalized through the incorporation of Ni<sup>2+</sup> into tetrahedral coordination positions in the willemite, again substituting for the Zn<sup>2+</sup> ions. Parmalee & Harman (1973) note that in nickel-bearing Rb<sub>2</sub>O glasses in which Ni<sup>2+</sup> is in tetrahedral coordination, an indigo colour results.

Iron occurs as a colorant in both P4 and P5, preferring to be in the glaze rather than in the willemite crystals, which have

roughly half or less of the iron content of the glaze. This is consistent with the paler cream colour of the willemite crystals in P5 compared with the honey-coloured glaze. Clarkson (1992) states that iron oxide used as a colorant gives cream/brown in crystalline glazes. Parmalee & Harman (1973) note that ferric ions,  $\text{Fe}^{3+}$ , produce a brownish colour in tetrahedral coordination, but also note the fact that iron oxide additions to silicate melts can produce a wide variety of colours and shades. These explanations for the brown colour would explain what is seen in both P4 and P5, but confirmation that this is indeed the reason for the colours noted in P4 and P5 would require chemical analysis beyond the scope of the work presented here. Furthermore, it might well be expected that Fe enters the willemite structure primarily as  $\text{Fe}^{2+}$ , not  $\text{Fe}^{3+}$ , and this would have an influence on the colour taken by the willemite crystals.

The greenish colours of the willemite spherulites and the surrounding glaze in P3 are provided by copper ions, which have a preference to be in the glaze, but are also capable of being incorporated into the willemite crystals, presumably as  $\text{Cu}^{2+}$  in a tetrahedral coordination replacing  $\text{Zn}^{2+}$  ions. In general, copper can exist as both  $\text{Cu}^+$  and  $\text{Cu}^{2+}$  ions. Müller (1992) notes the preference of  $\text{Cu}^{2+}$  for octahedral coordination because of the Jahn–Teller effect stabilizing this over tetrahedral coordination.  $\text{Cu}^+$  prefers a linear arrangement, such as in  $\text{Cu}_2\text{O}$  (Battey, 1981; Müller, 1992). Parmalee & Harman (1973) attribute the colour of greenish-blue glazes to the presence of both  $\text{Cu}^+$  and  $\text{Cu}^{2+}$  in the glaze. However, as for P3, confirmation of the valence states and coordination of the copper ions in the willemite crystals and the glaze, and thus an explanation for the colours seen on P3, would require further, more detailed, chemical analysis than that which we have presented here.

The occurrence of spherulites as the preferred macroscopic morphology of the willemite crystals can be rationalized in terms of diffusion-limited aggregation (Keith & Padden, 1963; Fowler & Roach, 1996). The fibrous morphology taken by the willemite crystals as a consequence of their trigonal structure and the ability of such crystals to undertake 'small angle branching', in which two distinct daughters are able to emerge from the tip of a parent fibre at some small angle, are also relevant to the development of the spherulitic morphology (Keith & Padden, 1963). Partitioning of the chemical elements within the glaze between the glass and the crystals which form within the glaze requires diffusion. Thus, although experimentally it is well-known from the ceramic art and craft literature that crystalline glazes are quite fluid (Machtey, 1978; Covert, 1981; Schmitz, 1984; Dann, 1991; Clarkson, 1992; Creber, 1997; Malone, 1997; Ilsley, 1999; von Dassow, 2002; Shimbo, 2003), principally to control the number of sites where nucleation of the willemite crystals first occur, the diffusion rates of silicon and zinc away from and to growth sites at the end of the acicular willemite crystals, respectively, determine the growth rates of the willemite crystals within the spherulites. Crystallization in such systems is therefore

necessarily a relatively slow process, and this accords with the pottery literature on zinc-containing crystalline glazes. By comparison, the partitioning of other elements, such as Al, K, Ca and transition metals, will be a secondary effect when determining willemite crystal growth rates.

Overall, the microscopy and microanalysis of the crystalline glazes has produced results on the morphology of the spherulites and the partitioning of transition metal ions between the willemite and the glaze in line with expectation from the scientific literature and the ceramic art and craft literature. However, it is evident that there is yet more microscopy-based work using analytical transmission electron microscopes that could be undertaken on suitable samples of crystalline glaze, such as helping to establish how the small angle branching occurs in willemite, mapping at nanometre resolution the distribution of chemical elements near the willemite–glaze interfaces and determining the valence state of transition metal ions in the glaze and in the willemite. It is hoped that this paper will encourage such work to be undertaken.

## Conclusions

Using standard microstructural characterization techniques, crystalline glazes in the six artefacts examined in this work have all been shown to consist of macroscopic spherulites made up of a large number of acicular willemite crystals within a silica-rich glaze. The texture adopted by the willemite crystals within a spherulite, whereby the [001] directions are parallel to the axes of the acicular crystals, can be confirmed both by X-ray diffractometry and using transmitted light polarized light microscopy with a sensitive tint. While it is preferable for X-ray diffraction work that flat surfaces should be used as samples, slightly curved samples can also produce satisfactory diffraction data. X-ray microanalysis in the scanning electron microscope further confirms that the crystals within the spherulites are willemite. Partitioning of chemical species between the willemite spherulites and the glaze can also be measured conveniently by X-ray microanalysis. This was found to be consistent with expectations from practical experience of crystalline glazes reported in the ceramic art and craft literature.

## Acknowledgements

We would like to thank Professors Giin-Shan Chen and Lindsay Greer and Dr Wong-Cheng Shih for the provision of examples of crystalline glazes used for this work. We would also like to thank David Vowles, Brian Barber and Andrew Moss for technical assistance.

## References

- Battey, M.H. (1981) *Mineralogy for Students*, 2nd edn. Longman, London.

- Clarkson, D. (1992) The crystal maze. *Ceramic Rev.* **137**, 27–31.
- Covert, C. (1981) Crystalline glazes. *Ceramic Rev.* **71**, 26–28.
- Cox, K.G., Price, N.B. & Harte, B. (1988) *The Practical Study of Crystals, Minerals and Rocks*, revised, 1st edn. McGraw-Hill, London.
- Creber, D. (1997) *Crystalline Glazes*. A & C Black, London.
- Cullity, B.D. & Stock, S.R. (2001) *Elements of X-Ray Diffraction*, 3rd edn. Prentice Hall, Upper Saddle River, N.J.
- Dann, M. (1991) Crystalline glazes. *Ceramic Rev.* **128**, 36–39.
- von Dassow, S. (2002) Making crystals clear. *Pottery Making Illustrated*, **November/December**, 25–29.
- Deer, W.A., Howie, R.A. & Zussman, J. (1966) *An Introduction to the Rock Forming Minerals*. Longman, London.
- Ehringhaus, A. & Rose, H. (1923) Über die Abhängigkeit der relativen Dispersion der Doppelbrechung vom Atomgewicht. *Z. Kristallogr.* **58**, 460–477.
- Fowler, A.D. & Roach, D.E. (1996) A model and simulation of branching mineral growth from cooling contacts and glasses. *Min. Mag.* **60**, 595–601.
- Gaines, R.V., Skinner, H.C.W., Foord, E.E., Mason, B., Rosenzweig, A., King, V.T. & Dowty, E. (1997) *Dana's New Mineralogy: the System of Mineralogy of James Dwight Dana and Edward Salisbury Dana*, 8th edn. John Wiley & Sons, Inc, New York.
- Goddard, A. (1995) Crystal glaze. *New Scientist*, **147** (1984), 27–29.
- Goodhew, P.J., Humphreys, J. & Beanland, R. (2001) *Electron Microscopy and Analysis*, 3rd edn. Taylor & Francis, London.
- Ilsley, P. (1999) *Macro-Crystalline Glazes: The Challenge of Crystals*. The Crowood Press Ltd, Marlborough.
- Karasu, B., Çakı, M. & Turan, S. (2000) The development and characterisation of zinc crystal glazes used for Amakusa-like soft porcelains. *J. Eur. Ceram. Soc.* **20**, 2225–2231.
- Karasu, B., Çakı, M. & Yeşilbaş, Y.G. (2001) The effect of albite wastes on glaze properties and microstructure of soft porcelain zinc crystal glazes. *J. Eur. Ceram. Soc.* **21**, 1131–1138.
- Karasu, B. & Turan, S. (2001) Effect of cobalt oxide and copper oxide additions to zinc-containing soft porcelain glazes. *Am. Ceram. Soc. Bull.* **80** (9), 41–45.
- Karasu, B. & Turan, S. (2002) Effects of cobalt, copper, manganese and titanium oxide additions on the microstructures of zinc containing soft porcelain glazes. *J. Eur. Ceram. Soc.* **22**, 1447–1455.
- Keith, H.D. & Padden, F.J. (1963) A phenomenological theory of spherulitic crystallization. *J. Appl. Phys.* **34**, 2409–2421.
- Kingery, W.D., Bowen, H.K. & Uhlmann, D.R. (1976) *Introduction to Ceramics*, 2nd edn. John Wiley & Sons, New York.
- Klaska, K.-H., Eck, J.C. & Pohl, D. (1978) New investigation of willemite. *Acta Cryst.* **B34**, 3324–3325.
- Lee, C.C., Shen, P. & Lu, H.Y. (1989) Formation of willemite from powder mixture with TiO<sub>2</sub> addition. *J. Mater. Sci.* **24**, 3300–3304.
- Levin, E.M., Robbins, C.R. & McMurdie, H.F. (1964) *Phase Diagrams for Ceramists*. The American Ceramic Society, Columbus, Ohio.
- Machtey, M. (1978) Crystalline glazes. *Ceramic Rev.* **49**, 16–19.
- Malone, K. (1997) Crystalline alchemy. *Ceramic Rev.* **164**, 21–24.
- Müller, U. (1992) *Inorganic Structural Chemistry*. John Wiley & Sons, Chichester.
- Norton, F.H. (1937) The control of crystalline glazes. *J. Am. Ceram. Soc.* **20**, 217–224.
- Norton, F.H. (1970) *Fine Ceramics: Technology and Applications*. McGraw-Hill, New York.
- Norton, F.H. (1974) *Elements of Ceramics*. Addison-Wesley, London.
- Parmalee, C.W. & Harman, C.G. (1973) *Ceramic Glazes*. Cahnners Books, Boston.
- Paul, A. (1982) *Chemistry of Glasses*. Chapman & Hall, London.
- Rudhovskaya, N.V. & Mikhailenko, N.Yu (2001) Decorative zinc-containing crystalline glazes for ornamental ceramics (a review). *Glass and Ceramics*, **58**, 387–390.
- Schmitz, R. (1984) Crystalline glazes. *Ceramic Rev.* **88**, 10–11.
- Shimbo, F. (2003) *Crystal Glazes: Understanding the Process and Materials*, 2nd edn. Digitalfire Corporation, Medicine Hat, Alberta.
- Sun Dakhai, Orlova, L.A. & Mikhailenko, N.Yu (1999) Types and compositions of crystalline glazes (a review). *Glass and Ceramics*, **56**, 177–180.
- Taylor, J.R. & Bull., A.C. (1986) *Ceramics Glaze Technology*. Pergamon Press, Oxford.
- Tilley, R.J.D. (2000) *Colour and Optical Properties of Materials*. John Wiley & Sons, Chichester.
- Turan, S. & Karasu, B. (2001) The effect of copper oxide addition and the heat treatment temperature on the microstructure of zinc containing soft porcelain crystal glazes. *Inst. Phys. Conf. Ser.* **168**, 315–318.
- Waerenborgh, J.C., Figueiredo, M.O., Cabral, J.M.P. & Pereira, L.C.J. (1994) Temperature and composition dependence of the cation distribution in synthetic ZnFe<sub>y</sub>Al<sub>2-y</sub>O<sub>4</sub> (0 ≤ y ≤ 1) spinels. *J. Solid State Chem.* **111**, 300–309.
- Williamson, J. & Glasser, E.P. (1964) Crystallisation of zinc silicate liquids and glasses. *Phys. Chem. Glasses*, **5**, 52–59.
- Wilson, A.J.C., ed. (1995) *International Tables for Crystallography*, 4th revised edition, Vol. C. Kluwer Academic Publishers, Dordrecht.

Copyright of Journal of Microscopy is the property of Blackwell Publishing Limited and its content may not be copied or emailed to multiple sites or posted to a listserv without the copyright holder's express written permission. However, users may print, download, or email articles for individual use.